Examination of the Effectiveness of Mode Orthogonalisation and Filtering for Scattering Suppression in Antenna Measurements Through Computational Electromagnetic Simulation

Zhengrong Tian, Stuart Gregson
Department of Engineering, Materials and Electrical Science, National Physical Laboratory, Teddington, UK
Zhengrong.Tian@npl.co.uk, Stuart.Gregson@qmul.ac.uk

***Abstract*— Reflections in antenna measurement ranges generally comprise the most significant term within the overall uncertainty budget [1, 2]. For well over a decade now, a frequency domain mode filtering based measurement technique has been utilized to significantly reduce range reflections within antenna test systems [1, 3, 4, 5, 6, 7, 8]. More recently however, this technique has been adapted so that it could also be used with far-field and compact antenna measurement systems [9, 10, 1] with the technique being firmly rooted in conventional cylindrical near-field theory [1]. Although this family of techniques was initially intended to provide a means by which the lower frequency limit of operation of a given facility [3, 4] could be extended downwards to work effectively in applications where the operation would otherwise be impaired by the fixed physical size of the absorber and therefore predetermined electrical performance, these techniques have more recently been used very successfully to improve performance at the upper end of the frequency extent [11]. Although this technique has been extensively examined and verified empirically by means of range measurements, relatively little verification by means of computational electromagnetic simulation is available in the open literature [1, 12, 13, 14, 15]. In this paper, we developed an efficient computational electromagnetic (CEM) model of the measurement configuration, *i.e.* a digital twin, using a three-dimensional, full-wave CEM solver. The purpose of this is to construct an absolute truth-model to provide a firm basis for a detailed quantitative examination of the scattering suppression technique. The modelling technique is discussed in detail and initial results are presented which show very good agreement between the "true" far-field pattern of the antenna in free space and that of the far-field of the antenna when perturbed with the presence of a scatterer and applying the scattering suppression process.**

***Index Terms*—antenna, propagation, measurement, computational electromagnetic simulation, multipath suppression.**

I. INTRODUCTION

When taking antenna measurements indoors, the effects of scattered fields are typically minimized by covering the interior surfaces of the chamber, and as much of the measurement equipment as is practical, with RF absorbing material. This absorber is typically manufactured from open-cell carbon impregnated foam which is costly, bulky and has a performance that is commensurate with its physical, and therefore electrical, size. This means that it is generally tailored for use across only a specific, limited predetermined range of frequencies with inevitable degradation in reflectivity performance towards these limits and especially outside of this band. Thus, the accuracy and precision of a general purpose facility is to some extent [3, 4, 11] compromised at its frequency extremes. As a result of this, methods for extending the frequency band of operation of a given test system through mitigation of range multipath are attractive and have received considerable attention in the published literature [16, 17]. A significant amount of time, effort and ingenuity have been devoted towards identifying and then extracting range reflections from antenna measurements with these techniques calling upon: software or hardware time-gating, background pattern subtraction, spatial filtering, complex plane circular least squares fitting and signal encoding methodologies. However, frequency domain mode filtering and measurement based methods for clutter rejection have become perhaps the most widely encountered techniques with variants being developed for use with all forms of antenna pattern measurement systems [1]. Although these mode orthogonalisation and filtering based techniques have become far more widely deployed, when compared to the volume of experimentally based verification, CEM based verification has received comparatively little consideration in the published literature. The use of electromagnetic simulation and a digital twin enables a far greater degree of freedom and control in the way in which one may perturb a given, otherwise ideal, measurement configuration.

To achieve this, the key is to build a suitable model and select an appropriate full-wave solver with sufficient modelling accuracy, flexibility and efficiency to demonstrate the phenomena under investigation. The modelling used herein is ultimately intended for use in a full two-dimensional 4π steradian spherical near-field simulation, however the first stage is to acquire a far-field great circle pattern cut and to validate the one-dimensional far-field

pattern correction technique which is the focus of this paper. The difficulties encountered in constructing an appropriate CEM model and the resolution employed are presented and discussed. Careful consideration is given to the validation of each step within the range simulation to ensure a reliable and stable digital twin is achieved.

This paper presents the results of this simulation which is used to provide further verification of the existing far-field cylindrical mode orthogonalisation and filtering scattering suppression technique [1, 5, 6, 9, 10]. This paper concludes with a summary and presents an overview of the planned future work.

II. Overview of The Techniques

Electromagnetic (EM) fields radiating into a homogeneous, linear, sink and source free region of space can be expanded onto a set of elementary orthogonal vector mode functions. These mode functions together with their attendant complex amplitudes can be used to represent the electric and magnetic fields everywhere in space outside of the bounding surface over which those fields were matched [1, 11, 18]. To illustrate this, equation (1) and (2) show the EM fields represented using spherical and cylindrical wave expansion, respectively [1,18].

$$\vec{E}(\vec{r}) = \sum_{n=1}^{\infty} \sum_{m=-n}^{n} \left[B^{1mn} \vec{M}^{nm}(\vec{r}) + B^{2mn} \vec{N}^{nm}(\vec{r}) \right] \tag{1}$$

$$\vec{E}(\vec{r}) = \sum_{n=-\infty}^{\infty} \int_{-\infty}^{\infty} \left[B_n^1(\gamma) \vec{M}_{n\gamma}^{(1)}(\vec{r}) + B_n^2(\gamma) \vec{N}_{n\gamma}^{(1)}(\vec{r}) \right] d\gamma \tag{2}$$

Here the transverse magnetic (TM) and transverse electric (TE) vector waves, *i.e.* basis functions, are denoted by $\underline{M}$ and $\underline{N}$, with the associated complex mode amplitudes being denoted by B^s. Conversely, the B^s mode coefficients can be obtained from the electric fields by inverting (1) and (2) using mode orthogonality [1, 18]. The dummy variables m and n are the mode indices. In practice, the fields are necessarily represented by a finite set of truncated modes with the upper limit of the truncated mode index (N) being determined by r_0, the minimum radius of the sphere or cylinder, which is also referred to as the maximum radial extent (MRE) and the frequency [1,18]. As a rule-of-thumb, N can be determined from the sampling theorem using $N=k_0r_0+10$.

Here k_0 is the free-space wave factor: $k_0=2\pi/\lambda$ and r_0 is the MRE of the antenna under test (AUT), which is determined by the size of the AUT and also the relative position of the AUT with respect to the origin of the measurement coordinate system. The addition of 10 modes is a safety margin which depends upon the accuracy required. This is a general number that is appropriate in many cases, however, for electrically large measurements a bigger margin may become necessary.

A closer examination of the cylindrical wave expansion, as shown in Equation (2), reveals a very useful feature of the cylindrical theory. In contrast to the analogous spherical wave expansion, which requires knowledge of two tangential orthogonal electric field components over the complete spherical bounding surface to obtain the spherical mode coefficients, the cylindrical mode coefficients (CMCs) require far less information [1,9,10]. For the cylindrical case, in the far-field the field components and mode coefficients separate with the desired tangential electric field component on a great circle cut, depending upon only a single set of modes. Furthermore, it is possible to obtain a set of CMCs from a single one-dimensional far-field cut. This is a very useful and convenient feature which additionally enables the validation of the CEM model using a reduced set of samples. The details of the cylindrical scattering suppression process can be found presented within the open literature [6] and is only summarized here:

1) Acquire the far-field amplitude and phase pattern cut of an antenna when offset from the origin of the measurement coordinate system.
2) Translate the far-field to the origin by applying a phase correction to the measured pattern data [1]

$$\text{Phase Correction} = 2\pi Z_{offset} \frac{\cos(\theta)}{\lambda} \tag{3}$$

3) Compute the CMCs using an inverse one-dimensional fast Fourier transform (IFFT).
4) Apply a band-pass filter function to extract higher order modes that are not associated with the AUT. A variety of different windowing functions can be applied and the study of effectiveness of several of these is one of the purposes of this study. A conventional scattering suppression filtering function [19] as shown in Equation (4) was used for scattering suppression processing in this paper.

$$f_n = \begin{cases} 1 & \text{when } |n| \le n_{\max} \\ 0.5^{|n|-n_{\max}} & \text{elsewhere} \end{cases} \tag{4}$$

5) Compute the mode filtered, scattering suppressed, far-field antenna pattern cut using a one-dimensional fast Fourier transform (FFT).

The construction of a sophisticated full-wave three-dimensional CEM digital-twin of the far-field measurement enables the careful and precise verification of the effectiveness of this post-processing algorithm.

III. CEM Modelling, the Digital-Twin

A. The modelling strategem

The ultimate goal of the modelling work is to recreate the measurement configuration in the antenna test range using a general-purpose full-wave three-dimensional CEM solver to obtain the simulated field pattern over the full 4π steradian sphere, and this inevitably involves a huge amount of computational effort. Thus, it is essential to build a suitable model which is accurate, sensitive, flexible and

computationally efficient. The first step in the development of this model was to consider the one-dimensional far-field pattern correction case presented above. The transmission model can be seen presented in Fig. 1.

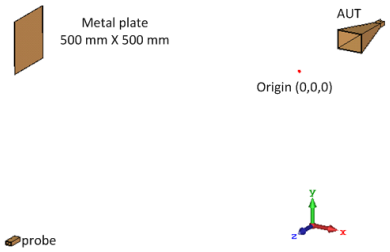

Fig. 1. Schematic representation of the three-dimensional transmission model showing the probe (remote source antenna), the offset AUT and the metallic plate which is introduced to perturb the system with spurious reflected fields.

In Fig. 1. the AUT is shown offset from the origin of the measurement coordinate system ($x = y = z = 0$). An open ended rectangular waveguide antenna is used as a probe in this schematic. A metal plate is introduced to perturb the system with the introduction of known scattering. The transmission scattering parameter S_{21} between the two waveguide ports of the AUT and the probe are simulated for each orientation of the AUT as it is sequentially rotated around the origin. In this way a very general replica, *i.e.* digital-twin, of the antenna range measurement can be constructed and used, not only for examination of the scattering suppression technique, as discussed herein, but also in principal probe effects and any other antenna measurement artifact of interest.

As discussed in the preceding section, the beauty of far-field cylindrical scattering suppression processing is that it can be applied to a single great circle far-field pattern cut without the need to have the knowledge of the complete far-field data set over the entire two-dimensional far-field spherical surface. This greatly reduces the simulation time and allows a detailed examination of the effect of the far-field cylindrical mode based scattering suppression technique which has not previously been possible. Although the transmission model is very useful, the field pattern acquired through the transmission model is not at infinite range, rather it is at a finite range. For the first stage modelling work, a field pattern at infinite range is desired and a far-field model is discussed in the following section.

B. Modelling validation

A WR75 standard gain horn (SGH) was selected to represent the AUT for the purpose of this simulation for several practical reasons. Firstly, the antenna geometry is comparatively simple and mechanically rigid and, as has been shown previously, very encouraging agreement has been attained between CEM simulation and actual range measurement. This reduces the number of potential sources of uncertainties when comparing the simulated data with the measured data and presents a significant advantage when compared to antennas comprising complex mechanical configurations containing dispersive materials. Secondly, as a scatterer is to be included within the model as a parametric change that is to be subsequently extracted, the model rapidly becomes an electrically large structure. The proprietary Integral Equation Solver within CST Microwave Studio was selected as it is a solver that is specifically intended to treat this sort of electrically large metallic structure. The essence of the scattering suppression technique is to measure the antenna with its aperture offset from the rotation centre by a certain known amount that is at least twice the conceptual minimum MRE, so that the authentic modes associated with the AUT and the higher order modes associated with the scatterer can be separated in the mode domain. Thus, the CEM model is required to recreate this situation by simulating the AUT with its aperture offset away from the rotation origin and acquire its far-field amplitude and phase at $\theta = 0°$ and $\phi = 0°$ for every point on the far-field cut which corresponds to each rotated position of the AUT, thus for N_θ points, N_θ individual simulations are required.

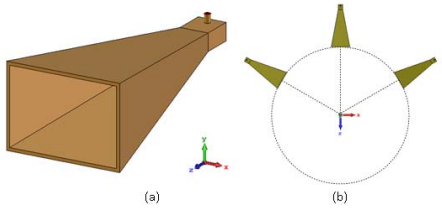

Fig. 2. (a) left. Perspective view of the EM model of a WR75 SGH with waveguide to coax transition. (b) right. Plan view of an offset AUT at a series of different rotation angles with the aperture offset from the rotation centre.

Fig. 2 (a) shows the perspective view of the model for a WR75 SGH. Fig. 2 (b) illustrates the AUT when offset along the Z axis and rotated to a series of different θ positions with the rotation centre located at the origin. Here, it is worth noting that the SGH was modelled with a waveguide to coax transition. In addition to improving the accuracy of the model, the auxiliary reason for this is due to the fact that both the time domain solver and integral equation solver require the waveguide port be aligned with a Cartesian axis. When the antenna is rotated to different θ angles, as shown in Fig. 2 (b), the waveguide section and port does not align to the *x*, *y*, *z* axis. For the case of the time-domain solver this means that the simulation cannot be run and in the case of the integral equation solver very poor results are obtained. Conversely, the frequency domain solver can accommodate a waveguide port which is not aligned to the Cartesian axis, however it is not computationally efficient for large electrical problems such as the one under consideration here. One approach that can be used to overcome this problem is to include a waveguide to coax transition so that as the AUT is rotated, the coax port will remain normal to the *y*-axis of the model.

As mentioned in the previous section, the modelling will involve the simulation of the offset antenna at a series of different rotation angles with the far-field exported at $\theta = 0°$

and $\phi = 0°$. A macro was developed so as to automatically generate the modelling file for each rotation position. A second macro was developed to export the far-field data at $\theta = 0°$ and $\phi = 0°$. To ensure both the model and the macros work correctly, simulations were initially run without the scatterer. Thus, the SGH was first simulated to obtain its far-field pattern without any rotation using both the time-domain and the integral equation solver. The resulting simulated far-field patterns were found to agree with one another, providing confidence that reliable data had been obtained. The simulation was then run for the rotated AUT case as illustrated in Fig. 2 (b) above with the far-field at $\theta = 0°$ and $\phi = 0°$ being extracted for each rotation case. These data sets were then combined together to form the great circle far-field pattern of the offset AUT. One critical setup when exporting the far-field point for each rotation case was to specify the far-field origin correctly. The far-field origin should be coincident with the rotation origin so that there is single consistent phase reference for each rotation case. If the model is configured correctly, clearly we can expect to obtain the same amplitude pattern from the two simulation methods. The comparison results can be seen presented in Fig. 3 (a) which confirmed this. Here, the thick green trace denotes the far field of the rotated AUT. Conversely, the conventionally simulated far-field pattern of the SGH is plotted in dark blue and constitutes the reference.

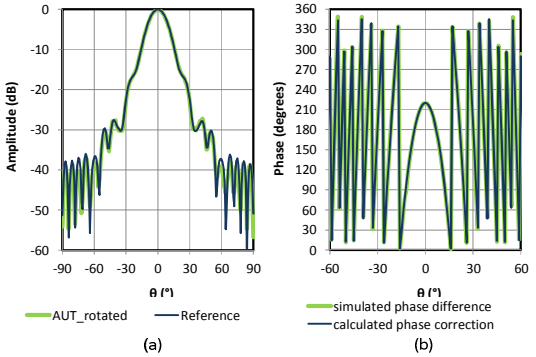

Fig. 3. Results comparison at 13 GHz: (a) amplitude; (b) phase difference

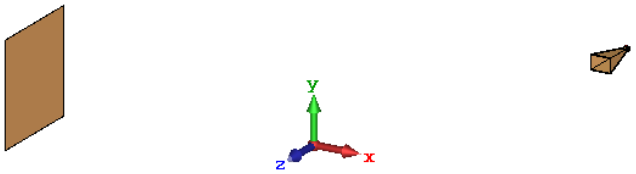

Fig. 4. AUT with a scattering plate (perspective view).

The phase pattern obtained from the two simulations should differ by the amount determined by the size of the physical offset and the simulation frequency as expressed by Equation (3). Fig. 3 (b) shows the simulated phase difference and the predicted phase difference. Here, it can be seen that the two patterns agree very well and this validates the underlying modelling strategy. In order that the scattering suppression technique presented above could be verified, the simulation was rerun, only this time a reflecting plate was introduced into the simulation. The results of this simulation are presented below in the following section.

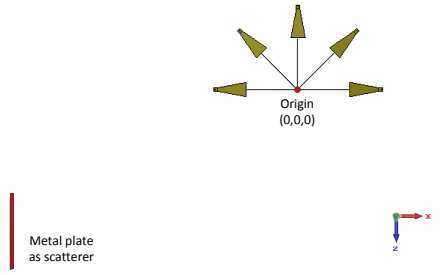

Fig. 5. Offset AUT with scatterer at different rotation position (plan view).

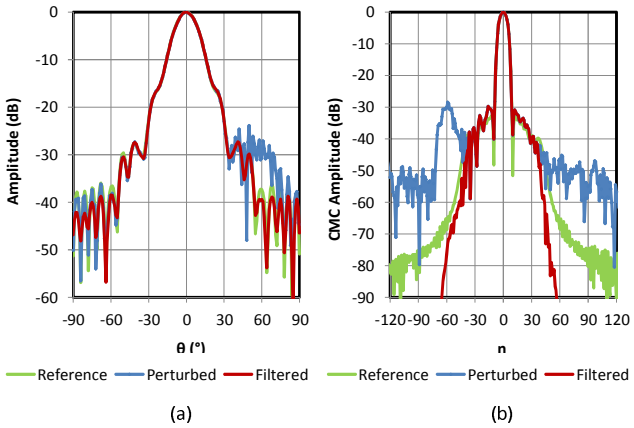

Fig. 6. (a) Amplitude of far field pattern with and without scattering suppression with far field pattern at 13 GHz of the horn antenna as reference; (b) Amplitude of the cylindrical mode coefficient (CMC) of the AUT with and without filtering compared with that of the horn antenna in free space.

IV. Results of Scattering Simulation

A square metallic plate 500 mm by 500mm was introduced into the model and used as a large scatterer. This arrangement is shown schematically in Fig. 4. Here, the centre of the reflecting plate was located at (-2000 mm, 0 mm, 1000 mm) and was used to simulate a highly exaggerated scatterer. The AUT was offset by 360 mm from the rotation origin (0, 0, 0). Fig. 5 illustrates the model for the offset AUT at different rotation angles with the scatterer in place. For each rotation position, the far-field of the combined structure, including both the rotated offset antenna and the scatterer, was simulated.

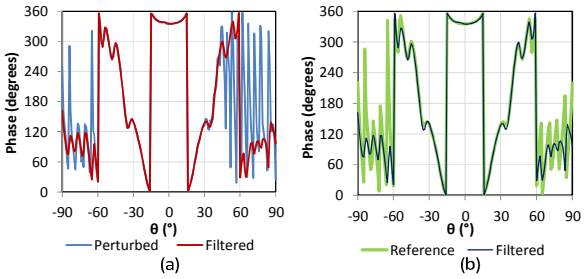

Fig. 7. Phase comparison: (a) comparison between before and after filtering; (b) filtered phase with simulated far field phase as reference.

Clearly, although the CEM simulation will provide the far-field pattern of the combined structure over the full 4π steradian far-field sphere, only the point at $\theta = 0°$ and $\phi = 0°$ is of interest here, as it is this single point that is used to populate the simulated "measured" far-field pattern cut. In Fig. 6 (a), the green trace denotes the free-space far-field amplitude pattern of the AUT as computed in this manner and this is plotted in the background and is used as the absolute truth-model. The blue trace denotes the simulated perturbed far-field pattern with the scatterer present. The simulated perturbed far-field pattern is then filtered using the conventional scattering suppression filter as described above with the mode-filtered amplitude pattern plotted in red. From inspection, it can be seen that the scattering due to the presence of the metallic plate has been effectively removed with the resulting pattern agreeing well with the reference data set. By way of a further illustration, Fig. 6 (b) compares the amplitude of the cylindrical mode coefficients of the free space horn antenna, the antenna with the scatterer before and after filtering. Here, it is clear that the modes associated with the metallic plate are displaced towards higher mode indices meaning that the mode filtering effectively extracts their influence from the mode-filtered far-field antenna pattern.

Lastly, Fig. 7 compares the reference phase pattern of the AUT in the free space, with and without the scatter with the mode filtered pattern, *i.e.* before and after scattering suppression processing. Again, very encouraging agreement can be seen between the free space reference phase pattern and the mode filtered phase pattern.

V. Summary and Conclusions

A full wave three-dimensional CEM model has been constructed and validated which can be used to recreate the far-field antenna pattern measurement configuration in a cylindrical and spherical scanning system. A metallic plate was introduced into the model and the perturbed far-field of the AUT with the scatterer was computed. Through far-field cylindrical scattering suppression processing, the scattering effect due to the presence of the scatterer was effectively removed, which was verified by comparison with the simulated far-field of the AUT in free-space without the scatterer. The reported study established a suitable working CEM-based digital-twin which emulates the antenna test configuration. Further work will include acquiring the simulated far-field data over the full sphere, and to examine and explore various windowing functions based on the simulated data. The general purpose model can be used to simulate spherical near-field measurement configurations, further enhancing the utility of the model.

Acknowledgment

The authors gratefully acknowledge the funding support provided by the UK National Measurement System and the Department for Business, Energy and Industrial Strategy (BEIS) that enabled the work that this paper presents.

References

[1] C.G. Parini, S.F. Gregson, J. McCormick, D. Janse van Rensburg, "Theory and Practice of Modern Antenna Range Measurements", IET Press, 2014, ISBN 978-1-84919-560-7.

[2] A.C. Newell, "Error Analysis Techniques for Planar Near-field Measurements", IEEE Transactions on Antennas and Propagation, vol. AP-36, pp. 754-768, June 1988.

[3] G.E. Hindman, A.C. Newell, "Reflection Suppression in a large spherical near-field range", AMTA 27th Annual Meeting & Symposium, Newport, RI, October. 2005.

[4] G.E. Hindman, A.C. Newell, "Reflection Suppression To Improve Anechoic Chamber Performance", AMTA Europe 2006, Munch, Germany, March 2006.

[5] S.F. Gregson, A.C. Newell, G.E. Hindman, "Reflection Suppression In Cylindrical Near-Field Antenna Measurement Systems – Cylindrical MARS", AMTA 31st Annual Meeting & Symposium, Salt Lake City, UT, November 2009.

[6] S.F. Gregson, A.C. Newell, G.E. Hindman, "Reflection Suppression in Cylindrical Near-Field Measurements of Electrically Small Antennas", Loughborough Antennas & Propagation Conference, November, 2009.

[7] S.F. Gregson, A.C. Newell, G.E. Hindman, M.J. Carey, "Extension of the Mathematical Absorber Reflection Suppression Technique to the Planar Near-field Geometry", AMTA, Atlanta, GA, October, 2010.

[8] S.F. Gregson, A.C. Newell, G.E. Hindman, P. Pelland, "Range Multipath Reduction in Plane-Polar Near-field Antenna Measurements", AMTA, Seattle, October 2012.

[9] S.F. Gregson, B.M. Williams, G.F. Masters, A.C. Newell, G.E. Hindman, "Application of Mathematical Absorber Reflection Suppression To Direct Far-Field Antenna Range Measurements", AMTA, Denver, October 2011.

[10] S.F. Gregson, J. Dupuy, C.G. Parini, A.C. Newell, G.E. Hindman, "Application of Mathematical Absorber Reflection Suppression to Far-Field Antenna Testing", LAPC, Loughborough, November, 2011.

[11] S.F. Gregson, Z. Tian, "Comparison of Spherical and Cylindrical Mode Filtering Techniques for Reflection Suppression With mm-wave Antenna Measurements", IEEE Conference on Antenna Measurements and Application, September 2018.

[12] S.F. Gregson, A.C. Newell, G.E. Hindman, "Examination of Far-Field Mathematical Absorber Reflection Suppression Through Computational Electromagnetic Simulation", International Journal of Antennas and Propagation, Special Issue on Recent Advances in Near-Field to Far-Field Transformation Techniques, March 2012.

[13] S.F. Gregson, C.G. Parini, A.C. Newell, G.E. Hindman, "Examination of the Effectiveness of Far-field Mathematical Absorber Reflection Suppression in a CATR Through Computational Electromagnetic Simulation" EuCAP, Paris, 2017,

[14] S.F. Gregson, A.C. Newell, C.G. Parini, "Verification of Feed Spill-over Reduction using FF-MARS in a CATR Using Computational Electromagnetic Simulation", IEEE APS, San Diego, July, 2017

[15] S.F. Gregson, C.G. Parini, A.C. Newell, "Examination of the Effectiveness of Far-field Mathematical Absorber Reflection Suppression in a CATR Through Electromagnetic Simulation", IET Microwaves, Antennas & Propagation Journal, April 2018.

[16] O. M. Bucci, G. D'Elia, M. D. Migliore, "A General and Effective Clutter Filtering Strategy in Near-Field Antenna Measurements," Microwaves, Antennas and Propagation, IEE Proceedings, vol. 151, no. 3, pp. 227- 235, 21 June 2004.

[17] Doren W. Hess, "The IsoFilter™ Technique: Isolating an Individual Radiator from Spherical Near-Field Data Measured in a Contaminated Environment", EuCAP 2007.

[18] J.E. Hansen, "Spherical near-field antenna measurements", Peter Peregrinus Ltd., London, United Kingdom, 1988.

[19] S.F. Gregson, A.C. Newell, P.N. Betjes, C.G. Parini, "Verification of Spherical Mathematical Absorber Reflection Suppression in a Combination Spherical Near-Field and Compact Antenna Test Range", 39th AMTA Annual Meeting and Symposium, Atlanta, Georgia, USA, October 15-20, 20017.